Molecular Biology of the Cell
Vol. 21, 354–368, January 15, 2010

# Induction of a Massive Endoplasmic Reticulum and Perinuclear Space Expansion by Expression of Lamin B Receptor Mutants and the Related Sterol Reductases TM7SF2 and DHCR7

**Monika Zwerger,* Thorsten Kolb,* Karsten Richter,* Iakowos Karakesisoglou,† and Harald Herrmann***

*Department of Molecular Genetics, German Cancer Research Center, 69120 Heidelberg, Germany; and †School of Biological and Biomedical Sciences, University of Durham, Durham DH1 3LE, United Kingdom

Submitted August 28, 2009; Revised November 13, 2009; Accepted November 17, 2009
Monitoring Editor: M. Bishr Omary

**Lamin B receptor (LBR) is an inner nuclear membrane protein involved in tethering the nuclear lamina and the underlying chromatin to the nuclear envelope. In addition, LBR exhibits sterol reductase activity. Mutations in the *LBR* gene cause two different human diseases: Pelger-Huët anomaly and Greenberg skeletal dysplasia, a severe chrondrodystrophy causing embryonic death. Our study aimed at investigating the effect of five LBR disease mutants on human cultured cells. Three of the tested LBR mutants caused a massive compaction of chromatin coincidental with the formation of a large nucleus-associated vacuole (NAV) in several human cultured cell lines. Live cell imaging and electron microscopy revealed that this structure was generated by the separation of the inner and outer nuclear membrane. During NAV formation, nuclear pore complexes and components of the linker of nucleoskeleton and cytoskeleton complex were lost in areas of membrane separation. Concomitantly, a large number of smaller vacuoles formed throughout the cytoplasm. Notably, forced expression of the two structurally related sterol reductases transmembrane 7 superfamily member 2 and 7-dehydrocholesterol reductase caused, even in their wild-type form, a comparable phenotype in susceptible cell lines. Hence, LBR mutant variants and sterol reductases can severely interfere with the regular organization of the nuclear envelope and the endoplasmic reticulum.**

## INTRODUCTION

The nuclear envelope (NE) is composed of the inner nuclear membrane (INM) and the outer nuclear membrane (ONM). The latter is contiguous with the endoplasmic reticulum (ER). Both membranes are separated by a gap of 30–50 nm, the perinuclear space (PNS), and fuse at the pore membranes where nuclear pore complexes (NPC) are embedded (Lusk *et al*., 2007). The nuclear lamina is a filamentous protein meshwork located closely underneath the INM (Dwyer and Blobel, 1976). It is mainly composed of nuclear intermediate filament proteins, i.e., A- and B-type lamins (Gruenbaum *et al*., 2005; Stewart *et al*., 2007). Lamin B receptor (LBR) was initially identified in chicken as a lamin B-binding protein residing in the INM (Worman *et al*., 1988). Since then, LBR orthologues have been characterized in various species ranging from *Drosophila melanogaster* to humans (Ye and Worman, 1994; Gajewski and Krohne, 1999; Wagner *et al*., 2004).

Human LBR contains 615 amino acids and is composed of two principal subdomains: The 208 residue hydrophilic N-terminal domain and the 407 residue hydrophobic C-terminal domain. The amino terminus faces the nucleoplasm and interacts with both B-type lamins and chromatin in a cell cycle-dependent manner (Pyrpasopoulou *et al*., 1996) as well as with chromatin-associated proteins such as heterochromatin protein 1 (HP1) (Ye *et al*., 1997), HA95 (Martins *et al*., 2000), and the methyl-CpG binding protein MeCP2 (Guarda *et al*., 2009). The latter authors suggested that LBR plays a pivotal role in heterochromatin assembly and maintenance. The C-terminal domain has been suggested to harbor eight transmembrane segments, with the C-terminus facing the nucleoplasm (Ye and Worman, 1994). Interestingly, the C-terminal domain shares high sequence homology with various sterol reductases from yeast to humans (Holmer *et al*., 1998). Accordingly, rescue experiments with C14-sterol reductase-deficient yeast strains confirmed that human LBR has 3$\beta$-hydroxysterol $\Delta$14-reductase activity (Silve *et al*., 1998). Because the postsqualene part of cholesterol biosynthesis takes place in the ER, it is not clear whether LBR acts as a sterol reductase only in the ER where it is synthesized or whether it is accessible for sterol metabolites also at the INM (Bennati *et al*., 2008).

Two other human sterol reductases, transmembrane 7 superfamily member 2 (TM7SF2) and 7-dehydrocholesterol

This article was published online ahead of print in *MBC in Press* (http://www.molbiolcell.org/cgi/doi/10.1091/mbc.E09–08–0739) on November 25, 2009.

Address correspondence to: Harald Herrmann (h.herrmann@dkfz.de).

Abbreviations used: CV, cytoplasmic vacuole; DHCR7, 7-dehydrocholesterol reductase; ER, endoplasmic reticulum; INM, inner nuclear membrane; LBR, lamin B receptor; LINC, linker of nucleoskeleton and cytoskeleton; NAV, nucleus-associated vacuole; NE, nuclear envelope; NPC, nuclear pore complex; ONM, outer nuclear membrane; PHA, Pelger-Huët anomaly; PNS, perinuclear space; TM7SF2, transmembrane 7 superfamily member 2.

reductase (DHCR7), are located at the ER and function at distinct steps of the cholesterol biosynthesis pathway (Bennati *et al*., 2006; Porter, 2008). LBR shares significant sequence homology with both of these enzymes, its C-terminal domain is 58% identical to TM7SF2 and 37% identical to DHCR7 (Holmer *et al*., 1998). In contrast to these sterol reductases, LBR harbors a unique N-terminal domain engaged in lamin binding and the structural organization of heterochromatin. In essence, LBR is a dual-function protein.

Ever since the first mutation in the NE protein emerin has been demonstrated to cause human disease, a broad spectrum of disease-causing mutations in various NE proteins has been described, including LBR, MAN1, LAP2$\alpha$, ZMPSTE24, nesprin-1, and lamins (Worman and Bonne, 2007). A large subset of these "envelopathies" comprises diseases caused by mutations in the *LMNA* gene encoding lamin A/C. But also for *LBR*, more than a dozen disease-related mutations have been described previously (Hoffmann *et al*., 2002; Best *et al*., 2003). These mutations can lead to Pelger-Huët anomaly (PHA) or to Greenberg skeletal dysplasia. PHA in the heterozygous state is a mild condition in which the granulocytes of affected individuals display hypolobulated nuclei. Immunoblot analysis of lymphoblastoid cells from heterozygous patients displayed approximately half of the wild-type LBR amount compared with control cells, whereas no mutated protein was detected. Apart from the abnormal nuclear morphology, no other clinical symptoms have been described in the heterozygous state. In one case of diagnosed PHA homozygosity with a splice site mutation, no mutant protein was detected but only trace amounts of normally spliced ("wild-type") LBR. This homozygous patient presented with mental retardation and disproportionate body stature, and his neutrophils had round, nonsegmented nuclei (Hoffmann *et al*., 2002).

Greenberg skeletal dysplasia is an autosomal recessive, severe chondrodystrophy characterized by fetal hydrops, abnormal chondro-osseous calcification and lethality of the fetuses (Oosterwijk *et al*., 2003; Waterham *et al*., 2003). Although elevated levels of an abnormal cholesterol precursor were detected in skin fibroblasts of an affected fetus, it was suggested that this disease represents an envelopathy rather than a defect in the cholesterol biosynthesis pathway (Waterham *et al*., 2003; Wassif *et al*., 2007).

Hardly anything is known about the molecular mechanisms leading to these diseases, and tissue material of Greenberg skeletal dysplasia affected fetuses is rare. Furthermore, because LBR is a dual-function protein, mutations might interfere with different cellular processes, such as cholesterol biosynthesis, NE function, and chromatin structure.

The purpose of our study was to investigate the cellular effects that are associated with the expression of human LBR disease mutants. We demonstrate that mutations in LBR can strongly affect the organization of NE components and the nuclear structure of cultured cells.

## MATERIALS AND METHODS

### Cell Lines

The following cell lines were used in this study: A431 (epidermoid carcinoma of the skin), HeLa clone 6 (cervical adenocarcinoma), MCF7 (adenocarcinoma of mammary gland), PLC/PRF/5 (liver hepatoma), U2OS (osteosarcoma), and T98G (glioblastoma) (ATCC CRL-1555, CCL-2, HTB-22, CRL-8024, HTB-96, and CRL-1690). Cells were maintained according to the American Type Culture Collection (Manassas, VA) guidelines. For live cell imaging experiments, cells were plated on two-well Lab-Tek chambers (catalog no. 155379; Nalge Nunc International, Rochester, NY) in DMEM without phenol red and with 25 mM HEPES (catalog no. 21663; Invitrogen, Carlsbad, CA), 10% fetal calf serum and 2 mM L-glutamine. All transfection experiments were performed using the FuGENE 6 transfection reagent (Roche Diagnostics, Mannheim, Germany) following the manufacturer's instructions. For stable cell lines, U2OS cells were transfected and after 24 h treated with 1.5 mg/ml G418 (catalog no. G1001; Research Laboratories, Plymouth Meeting, PA) for selection of transfection-positive stable cells.

### Chemicals

Nocodazole and latrunculin B (Sigma-Aldrich, St. Louis, MO) were dissolved in dimethyl sulfoxide (DMSO). For disassembly of microtubules or actin filaments, cells were treated for 2 h with 5 $\mu$M nocodazole or 2 $\mu$M latrunculin B, respectively. For induction of ER stress, cells were treated with 10 $\mu$g/ml tunicamycin (catalog no. 654380; Merck, Darmstadt, Germany) for 6 h. To detect transcriptional activity, cells were treated with 5 mM of the cell permeable 5-fluorouridine (5-FU; catalog no. F1530, Sigma-Aldrich) dissolved in double-distilled $H_2O$. Transcription was inhibited by treatment of cells for 8 h with 5 mM actinomycin D (catalog no. A9415; Sigma-Aldrich) dissolved in DMSO. In all experiments involving nocodazole, latrunculin B or actinomycin D, equivalent amounts of the DMSO solvent were added to control cultures. No effects of the solvent alone could be detected.

### Plasmids

For transfection experiments, the coding sequence of human LBR was amplified using specific primers and the plasmid QY-1 as a template (Ye and Worman, 1994). Polymerase chain reaction (PCR) fragments were then digested via BglII/XhoI and ligated in pEYFP-C1 or mCherry-C1 (Clontech, Mountain View, CA). Cloning into pEGFP-N1 (Clontech)—for the expression of the LBR constructs without any tag—was performed using a stop codon for termination and the XhoI/BamHI restriction sites. The LBR disease mutant constructs were designed based on five human mutations (Table 1 and Figure 1).

For amplification of human TM7SF2 (alternate names D14SR, SR-1; RefSeq accession NP_003264), a plasmid containing its coding sequence was provided by Rita Roberti (University of Perugia, Perugia, Italy). The amplified coding sequence was cloned into pEYFP-C1 via BspEI/SalI or with a stop codon in pEGFP-N1 via BglII/SalI restriction sites. DHCR7 (alternate name SR-2, RefSeq accession NP_001351) was amplified from a cDNA library (PCR-Ready Human Skeletal Muscle cDNA; catalog no. 3334, Ambion, Austin, TX) and cloned into pEYFP-C1 via BspEI/SalI. The signal peptide-green fluorescent protein (SP-GFP) construct contains the coding sequence of the first 21 residues of human torsinA (Liu *et al*., 2003) cloned XhoI/NheI into pcDNA3.1 followed by the GFP sequence (NheI/EcoRI). Lamin B2 was amplified and cloned into pEYFP-C1 via BspEI/EcoRI. The Nup153-YFP construct was generated from NUP153-GFP (provided by Birthe Fahrenkrog, Universität Basel, Biozentrum, Basel, Switzerland), by replacement of GFP by yellow fluorescent protein (YFP) using the AgeI/BrsGI restriction sites. For induction of apoptosis, cells were transfected with a vector containing the proapoptotic murine *Bax* gene (provided by Otto Mannherz, DKFZ, Heidelberg, Germany).

### Bradford Protein Assay

A431, HeLa, MCF7, PLC, U2OS, and T98G cells were trypsinized, counted in a hemocytometer, and $3 \times 10^6$ cells were lysed in 8 M urea, 5 mM Tris, pH 7.5, 0.2% Nonidet P40, and 1 $\mu$l/ml Benzonase (catalog no. 71205; Novagen, Madison, WI) for 15 min at room temperature. Protein concentrations of the lysates were analyzed based on the Bradford method (Bradford, 1976) by using the Bio-Rad Protein Assay (catalog no. 500-0006; Bio-Rad Laboratories, Hercules, CA) and bovine serum albumin as a standard.

### Immunoblot Analysis

For preparation of total cell lysates, trypsinized cells from late logarithmically growing cultures were counted in a hemocytometer and boiled in Laemmli sample buffer as described previously (Zwerger *et al*., 2008). Total protein lysates, human brain tissue lysate (catalog no. PK-AB718-1303, PromoCell, Heidelberg, Germany) and molecular weight markers (catalog no. P7702; New England Biolabs, Frankfurt, Germany) were subjected to gel electrophoresis using 10% polyacrylamide gels (Laemmli, 1970) or 4–20% precast gels (catalog no. 161-1105; Bio-Rad Laboratories). Gels were electroblotted onto polyvinylidene difluoride membranes (Millipore, Billerica, MA) by using a tank transfer system in transfer buffer (25 mM sodium borate, pH 8.8, 1 mM EDTA, and 0.1 mM dithiothreitol). Membranes were probed with the following primary antibodies: guinea pig serum against LBR at a dilution of 1:1000 (Cohen *et al*., 2008), rabbit monoclonal anti-LBR (catalog no. 1398-1; Epitomics, Burlingame, CA), mouse monoclonal LBR raised against the last 15 amino acids of the protein (LBR KLH-19, undiluted), mouse monoclonal anti-lamin B2 at a 1:10 dilution (clone X223; catalog no. 65147C, Progen, Heidelberg, Germany), rabbit anti-LC3 serum at 1:500 (catalog no. NB100-2331; Novus Biologicals, Littleton, CO), mouse monoclonal anti-$\beta$-actin at dilution 1:20,000 (catalog no. A5441; Sigma-Aldrich), and mouse monoclonal anti-$\alpha$-tubulin at dilution 1:10,000 (catalog no. T5168; Sigma-Aldrich). Mouse monoclonal anti-lamin A/C (LaZ-1) (Geiger *et al*., 2008) and anti-lamin B1 (clone

**Table 1.** Human *LBR* mutations and the corresponding mutant proteins

| Mutation | Associated disease | Nucleotide change | Changes on protein level | Simplified designation | Reference |
|---|---|---|---|---|---|
| Nonsense | Heterozygous PHA | 1129C→T | Amino acid substitution Arg377X | LBR (1-376) | Hoffmann *et al.* (2002) |
| Frameshift | Heterozygous PHA | 1173delC | Amino acid substitution Gly392Asp, Leu393X | LBR (1-392) | |
| Nonsense | Heterozygous PHA | 1308G→A | Amino acid substitution Trp436X | LBR (1-435) | |
| Splice acceptor | Heterozygous and homozygous PHA | IVS12-5-10del | Loss of exon 13 | LBR (Δ523-563) | |
| Nonsense | Greenberg skeletal dysplasia | 1599–1605 TCTTCTA→CTAGAAG substitution | Amino acid substitution Leu534X | LBR (1-533) | Waterham *et al.* (2003) |

Expression levels of mutated proteins within affected individuals are largely unknown. Only lymphoblastoid cells of patients carrying the IVS12-5-10del mutation were analyzed, and no mutant protein was detected. Whether the mutant protein is expressed in cells from other tissues is not known.

#102) were generated in collaboration with H. Zentgraf (DKFZ) and used 1:1 diluted. As secondary antibodies, peroxidase-coupled goat anti-guinea pig, goat anti-mouse, and goat anti-rabbit immunoglobulin Gs (Jackson ImmunoResearch Laboratories, West Grove, PA) were used. All immune reactions were carried out in 10 mM Tris-HCl, pH 8.0, 150 mM NaCl, and 0.05% Tween 20, with 5% milk powder at room temperature.

### *Fluorescence and Immunofluorescence Microscopy*

For fluorescence microscopy, cells were grown on coverslips and fixed 24 h after transfection using formaldehyde, or, alternatively, methanol and acetone as described previously (Zwerger *et al*., 2008). The following primary antibodies were used for immunofluorescence microscopic analysis: mouse monoclonal anti-β-actin at dilution 1:2000 (catalog no. A5441; Sigma-Aldrich), monoclonal anti-α-tubulin at dilution 1:1000 (catalog no. T5168; Sigma-Aldrich), mouse monoclonal anti-calnexin at 1:100 dilution (catalog no. C7617; Sigma-Aldrich), mouse monoclonal anti-lamin A/C (LaZ-1, undiluted), mouse monoclonal anti-LBR C-term (LBR KLH-19, undiluted), guinea pig serum against emerin at dilution 1:500 (Dreger *et al*., 2002), rabbit anti-Sun1 at 1:100 (anti-UNC84A from Sigma/Atlas Antibodies, Stockholm, Sweden; catalog no. HPA008346), rabbit anti-Sun2 at 1:1000 (from Didier Hodzic, Washington University School of Medicine, St. Louis, MO), mouse monoclonal K20-478 anti-nesprin-2 giant at 1:50 (from Angelika Noegel, University of Cologne, Cologne, Germany), mouse monoclonal ab414 directed against NPC proteins at 1:1000 dilution (from Birthe Fahrenkrog, Universität Basel, Biozentrum), a polyclonal anti-TM7SF2 serum at 1:100 (from Rita Roberti, University of Perugia; Roberti *et al*., 2002), and a monoclonal anti-5-bromo-2′-deoxyuridine (BrdU) antibody at 1:40 (NA20; Calbiochem, San Diego, CA). The secondary antibodies (Cy3-conjugated or Alexa 568-conjugated) were obtained from Jackson ImmunoResearch Laboratories, and Invitrogen, respectively, and diluted according to the suppliers' suggestions. For detection of apoptotic cells, the In Situ Cell Death Detection kit, TMR red (catalog no. 2156792; Roche Diagnostics) was used following the supplier's instructions.

Analysis of fixed specimens was performed by confocal laser scanning microscopy (model TCS-SP II; Leica Microsystems, Deerfield, IL). Optical sections were acquired with a 40x, 63x or a 100x oil-immersion objective, at pinhole-size 1 Airy. For live cell imaging, a DeltaVision Core microscope (Applied Precision, Issaquah, WA) equipped with a WeatherStation environmental control for constant temperature of 37°C was used. From 12 h on after transfection, cells were stained with Hoechst 33342, and four-dimensional image stacks of 16 × 0.5 μm every 5 min were acquired with a 60× oil-immersion objective. Images were deconvolved using the built-in SoftWoRx software (Applied Precision).

### *Image Analysis*

Image analysis for size measurements of vacuoles and nuclei in both fluorescence and electron microscopy micrographs was performed using ImageJ software (National Institutes of Health, Bethesda, MD).

### *Electron Microscopy*

For the ultrastructural investigation of the morphological changes occurring in U2OS cells upon expression of YFP-LBR (1-533), transfected cells were grown on cover slips. Ten and 24 h after transfection, cells were fixed in a mixture of 4% freshly prepared formaldehyde and 1% glutaraldehyde (EM-grade; Sigma-Aldrich) in phosphate-buffered saline (PBS, pH 7.2) for 1 h on ice, rinsed in PBS, and postfixed in 1% buffered $OsO_4$ for 30 min at room temperature. After washing steps in PBS and double-distilled water, dehydration of the sample was carried out in aqueous ethanol of increasing concentration, i.e., 30, 50, 70% (saturated with uranylacetate for en-bloc staining overnight) followed by 100% ethanol (3 times). The samples were then embedded in epoxy resin (Epon 812; Sigma-Aldrich) and polymerized at 60°C with resin-filled gelatin capsules inverted on top of the coverslips. The coverslips were subsequently removed by exposure to liquid nitrogen. Ultrathin sections at nominal thickness of 70 nm were prepared, poststained in aqueous lead citrate, and observed in a Philips 410 transmission electron microscope (FEI, Eindhoven, The Netherlands). Overview micrographs were recorded at a magnification of 3000×, detailed views at 17,000×, 31,000×, 38,000×, and 82,000×, by using a charge-coupled device camera (Bioscan 792; Gatan, Pleasanton, CA).

### *Sterol Analysis*

Lipid extraction of untransfected, YFP-LBR wild-type (wt) and YFP-LBR (1-533) transfected U2OS cells of confluent 60-mm dishes and subsequent sterol analysis were performed by Organobalance (Berlin, Germany), as reported previously (Veen *et al*., 2003).

### *ER Stress Detection Assay*

For detection of ER stress induction, cells were resuspended in TRIzol (catalog no. 15596-018; Invitrogen), and mRNA was purified using the RNeasy mini kit (catalog no. 74104; QIAGEN, Hilden, Germany). cDNA was produced from this mRNA with the help of Moloney murine leukemia virus reverse transcriptase and random pdN6 primers. The target cDNA was amplified using the Xbp-1 sense primer (5′-CTGGAACAGAAAGT-3′) and antisense primer (5′-CTGGGTCCTTCTGGGTAGAC-3′) in a PCR reaction with 35 cycles (30 s at 94°C, 30 s at 52°C, and 45 s at 72°C). For accurate detection of the PCR fragment lacking 26 nucleotides, PCR products were analyzed on a 3% agarose gel.

### *Detection of Transcriptional Activity Using 5-FU Incorporation*

U2OS cells were transfected with either YFP-LBR wt or YFP-LBR (1-533). 24 h after transfection, 5-FU (catalog no. F1530; Sigma-Aldrich) was added to the growth medium in a final concentration of 5 mM for 4 h. Incorporation of 5-FU into nascent RNA was detected by immunofluorescence analysis using antibodies specific for BrdU. Two control experiments were applied. First, actinomycin D (catalog no. A9415; Sigma-Aldrich) was added to the growth medium 20 h after transfection and 4 h before addition of 5-FU to the cells for 8 h at a final concentration of 5 mM. Second, after 5-FU incorporation, cells were fixed, and RNA was digested with 1 mg/ml RNase A (catalog no. 109169; Roche Diagnostics) for 30 min at room temperature.

## RESULTS

### *Different Human Cultured Cell Lines Express Variable Amounts of LBR and Lamins*

Because we wanted to investigate the effects of LBR disease mutations (Figure 1 and Table 2) on the organization of the NE, we first determined the content of endogenous LBR and

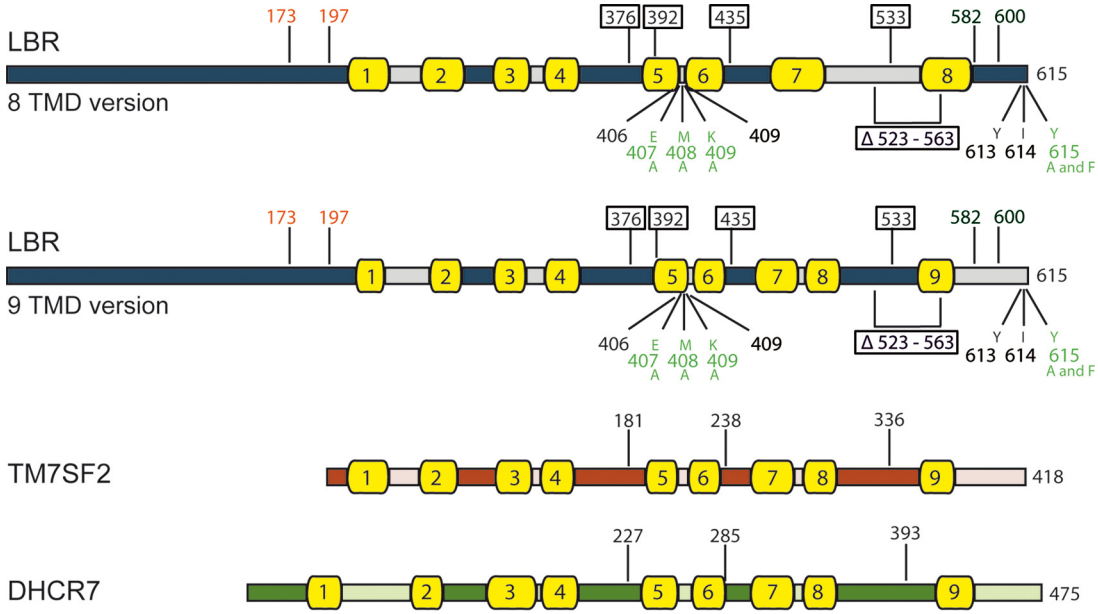


**Figure 1.** Structural organization of human LBR and the human sterol reductases TM7SF2 and DHCR7. Light colors indicate lumenal stretches, and dark colors indicate domains exposed to the nucleoplasmic or cytoplasmic part of the cell. Yellow barrels with black numbers represent transmembrane domains (TMD). The TMD prediction of Ye and Worman (1994) indicates eight TMD, whereas TMD prediction using the program *TMpred* (www.ch.embnet.org) calculates nine TMD for LBR. The predictions for TM7SF2 (Roberti *et al*., 2002) and for DHCR7 (Fitzky *et al*., 1998) reveal nine TMD for both proteins. In both cases, the *TMpred* prediction program was used. Black numbers indicate the amino acid length of LBR C-terminal truncations, and black numbers in boxes designate LBR variants that correspond to disease-related mutations described in PHA and Greenberg skeletal dysplasia patients. In TM7SF2 and DHCR7, black numbers indicate the site of C-terminal truncations that correspond to LBR disease mutants; red numbers specify the amino acid that N-terminally truncated LBR variants initiate with; and green numbers identify single amino acid changes introduced in the full-length LBR.

lamins in six cell lines derived from different human tissues, i.e., skin (A431), ovary (HeLa), breast (MCF7), liver (PLC), bone (U2OS), and brain (T98G) by immunoblot analysis of whole cell lysates (Figure 2A). We chose to compare the LBR and lamin content between equal cell numbers of the six cell lines. They all contain similar total protein levels, as reflected by the relatively constant amount of $\alpha$-tubulin detected in all samples and by measurement of total protein content (50–85 $\mu g/10^5$ cells; see legend for Figure 2). The highest LBR expression was encountered in PLC cells, whereas MCF7 cells contained only very low amounts. The other cell lines, A431, HeLa, U2OS, and T98G, had moderate LBR levels. All cell lines contained similar amounts of lamin B1. In contrast, the lamin B2 content varied drastically: A431, MCF7, and PLC cells expressed no or minimal amounts of lamin B2, whereas it was highly abundant in T98G cells. Also, the levels of lamins A and C as well as their ratio varied strongly. T98G cells displayed very high and comparable levels of both A-type lamins, whereas PLC cells lacked lamin A nearly completely but expressed significant amounts of lamin C. Taken together, we did not find any correlation between LBR and lamin levels in the cell lines investigated.

### *Expression of LBR wt in Human Cell Lines*

After transient overexpression of YFP-LBR wt, two phenotypes could be distinguished by fluorescence microscopy (Figure 3). In HeLa as well as in PLC cells, YFP-LBR wt localized to the NE and throughout the cytoplasm in a tubular pattern (Figure 3, A and B). In contrast, A431, MCF7, T98G, and U2OS cells strongly overexpressed the fusion protein, and large fluorescent aggregates formed within the cytoplasm, often intimately associated with the nuclear rim (Figure 3, C–F). Nevertheless, their formation apparently did not interfere with the nuclear architecture. Moreover, similar aggregates also formed in U2OS cells stably expressing YFP-LBR wt (Supplemental Figure S1). Hence, cells can propagate normally despite the existence of such cytoplasmic aggregates.

Because all original forms of GFP have been reported to exhibit a tendency for homodimerization at high expression levels (Zacharias *et al*., 2002), we replaced the YFP by the nondimerizing mCherry protein, which is a variant of the monomeric fluorescent protein mRFP (Campbell *et al*., 2002; Shaner *et al*., 2004). As expected, mCherry-LBR wt never formed aggregates in U2OS cells, even upon strong expression. Cytoplasmic localization was always in network-like patterns, similar to that observed in U2OS cells expressing low levels of YFP-LBR wt (Figure 3, G and H). In previous studies, endogenous expression of chicken LBR resulted in a more predominant NE localization of LBR in COS-7 cells (Soullam and Worman, 1993, 1995). The strong ER staining we observed upon LBR overexpression might reflect higher expression levels of the fusion protein in our study. It is well possible that the level of YFP-LBR wt expressed in our cells exceeds the capacity of the INM for protein incorporation, leaving a large fraction of the fusion protein within the ER membrane. An early study on LBR overexpression resulted in the formation of NE invaginations that differ from the organized smooth endoplasmic reticulum (OSER) structures we observed upon YFP-LBR overexpression (Supplemental Figure S1; Ellenberg *et al*., 1997). Notaby, however, Ellenberg and coworkers used a construct consisting of truncated human LBR (the N-terminal 238 residues) with only one transmembrane segment and hence missing most of the C-terminal domain of the protein (residues 239–615), followed by

**Table 2.** Constructs used for transfection experiments in human cell lines

| | LBR | TM7SF2 | DHCR7 |
|---|---|---|---|
| | LBR wt[a] | TM7SF2 wt[b] | DHCR7 wt |
| Disease | LBR (Δ523-563)[a] | | |
| mutations | LBR (1-533)[a] | TM7SF2 (1-336)[b] | DHCR7 (1-393) |
| | LBR (1-435)[a] | TM7SF2 (1-238) | DHCR7 (1-285) |
| | LBR (1-392)[a] | TM7SF2 (1-181) | DHCR7 (1-227) |
| | LBR (1-376)[a] | | |
| N-terminal | LBR (173–615) | | |
| truncations | LBR (197–615) | | |
| C-terminal | LBR (1-406) | | |
| truncations | LBR (1-409) | | |
| | LBR (1-582) | | |
| | LBR (1-600) | | |
| | LBR (1-613) | | |
| | LBR (1-614) | | |
| Point | LBR (E407A) | | |
| mutations | LBR (M408A) | | |
| | LBR (K409A) | | |
| | LBR (Y615A) | | |
| | LBR (Y615F) | | |

Note that point mutations were introduced to the full-length LBR. TM7SF2 and DHCR7 truncation constructs correspond to the LBR disease mutants in the same row. All constructs were generated N-terminally fused to YFP.

[a] These constructs were additionally generated with an N-terminal mCherry-tag instead of YFP as well as without tag.

[b] These constructs were additionally generated without tag.

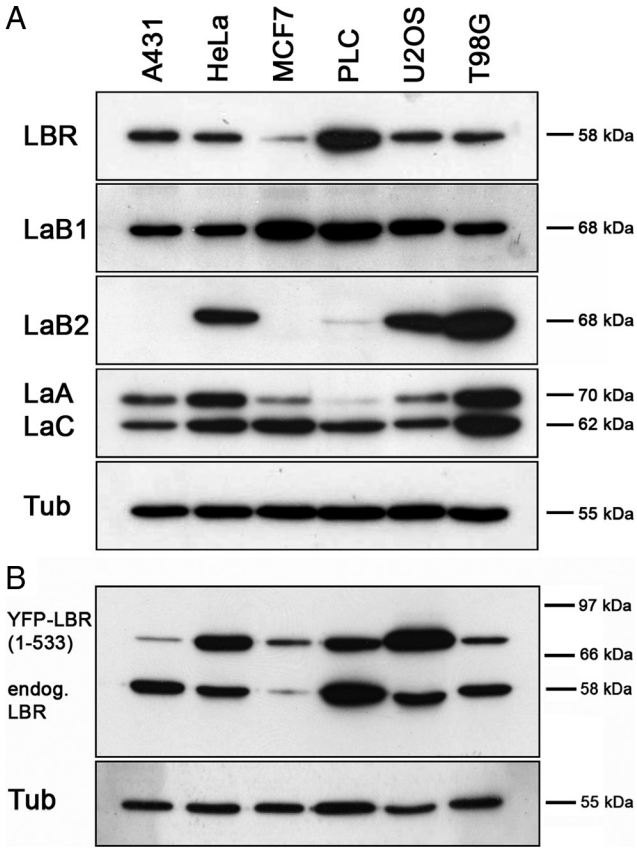


**Figure 2.** Quantitative immunoblot analysis of the content of LBR, lamin B1 (LaB1), lamin B2 (LaB2), lamin A/C (LaA and LaC), and α-tubulin (Tub) (A) as well as endogenous LBR, the transiently expressed mutant YFP-LBR (1-533), and α-tubulin (B) in the six human cultured cell lines designated above each lane. Total cell lysates representing $10^5$ (A) and $5 \times 10^4$ cells (B) were loaded per lane, respectively. Comparable protein content was confirmed by probing with an α-tubulin antibody and by directly determining the total protein content of $10^5$ cells, yielding 53.2 μg (A431), 57.2 μg (HeLa), 58.1 μg (MCF7), 84.9 μg (PLC), 50.1 μg (U2OS), and 78.4 μg (T98G) for the respective cell lines.

GFP in the perinuclear space. The presence of the entire C-terminal domain within the YFP-LBR wt construct we used and the different position of the fluorescent protein may explain the formation of OSER structures rather than NE invaginations.

### *Expression of the LBR Mutants (1-435), (Δ523-563), and (1-533) but Not (1-376) and (1-392) Leads to Nuclear Compaction and Development of Prominent Vacuoles*

We then investigated the expression of the five LBR mutant forms YFP-LBR (1-376), (1-392), (1-435), (Δ523-563), and (1-533) in all six cell lines analyzed above. In U2OS cells, we observed basically two different phenotypes (Figure 4): YFP-LBR (1-376) and YFP-LBR (1-392) localized at the NE with a varying number of fluorescent foci in the cytoplasm, similar to YFP-LBR wt. We never observed changes in nuclear structure or size with these constructs. In stark contrast, the fusion proteins YFP-LBR (1-435), YFP-LBR (Δ523-563), and YFP-LBR (1-533) were predominantly expressed in small accumulations in the cytoplasm and only low amounts of the fusion protein were detected at the NE (see inset in Figure 4C). The nuclear volume was severely reduced compared with that of untransfected cells. Large vacuole-like structures formed at one or few sites of the nucleus, such that nuclei became flattened at these sites (arrowheads in Figure 4, D and E). These areas contained no fusion protein and could be easily distinguished from the nucleus by their vacuous appearance with differential interference contrast (DIC) as well as with phase contrast microscopy (Figure 4, E′ and 4E″). We called these areas nucleus-associated vacuoles (NAVs). In their size, NAVs ranged from small areas adjacent to nuclei of normal appearance to large compartments adjoining strongly compacted nuclei. Concomitantly to the formation of NAVs, a large number of smaller vacuole-like structures appeared throughout the cytoplasm. We termed them cytoplasmic vacuoles (CVs). This phenotype was also observed in A431 and T98G cells but not in MCF7 and PLC cells upon expression of YFP-LBR (1-435), YFP-LBR (Δ523-563), and YFP-LBR (1-533). HeLa cells developed vacuoles to a much lower extent and size (data not shown). Most notably, the effect was independent of the expression level of the mutant protein. A431 and T89G express significantly lower levels of YFP-LBR (1-533) than PLC cells, but they display NAVs, CVs and compacted nuclei whereas PLC cells do not (Figure 2B). The effect was also independent of the fusion tag, as mCherry tagged or even untagged mutant LBR led to the same morphological abnormalities as those observed with the YFP-tagged versions (Supplemental Figures S2 and S3).

### *LBRs Amino Acids 407 and 615 and the Stretch between These Residues Are Critical for Vacuole Formation and Nuclear Compaction*

The previous experiments had shown that YFP-LBR (1-435) induced a dramatic size reduction of nuclei and the emergence of NAVs and CVs but that the shorter LBR mutants (1-376) and

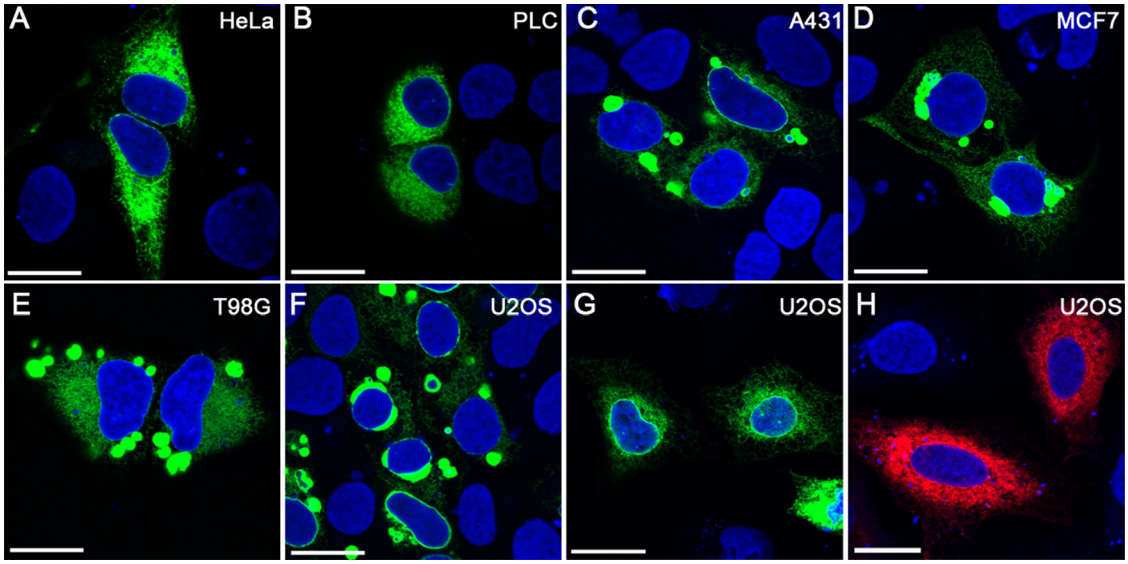


**Figure 3.** Expression patterns of fluorescent protein tagged LBR wt: YFP-LBR wt in HeLa (A), PLC (B), A431 (C), MCF7 (D), T98G (E), and U2OS (F and G) and of mCherry-LBR wt (H) in U2OS. (A, B, and G) On moderate expression, YFP-LBR wt localizes to the nuclear rim and in addition in a tubular network-like pattern to the cytoplasm. (C, D, E, and F) Higher expression of YFP-LBR wt causes the formation of large cytoplasmic aggregates, frequently associated with the nuclear rim. (H) With the fluorescence tag mCherry (a monomeric GFP variant) large aggregates—as seen with the YFP-tagged version—are absent. Chromatin was counterstained with DAPI (blue). Original images were collected with a 63× objective. Bar, 20 $\mu$m.

(1-392) did not. To examine the minimal LBR length capable to induce the aberrant phenotype, we generated further LBR truncations with a length between 392 and 435 aa. Thereby, we identified two constructs, YFP-LBR (1-406) and YFP-LBR (1-409), of which the first behaved like YFP-LBR wt and the second, carrying only three additional residues, induced nuclear compaction, NAVs, and CVs in U2OS cells (data not shown). We then mutagenized in the full-length LBR each of these three amino acids (E407, M408, and K409) separately to the neutral, nonpolar amino acid alanine, and we found that neither YFP-LBR (M408A) nor YFP-LBR (K409A) but only YFP-LBR (E407A) was effective in inducing the abnormal phenotype (data not shown). Furthermore, we demonstrated that YFP-LBR (1-533) caused nuclear compaction and vacuole formation, whereas YFP-LBR wt did not. In a next series of experiments we hence investigated YFP-tagged LBR variants truncated in the very C-terminal part of the protein between amino acids 533 and 615. These constructs lacked either the full C-terminal segment after the last transmembrane domain [33 residues, YFP-LBR (1-582)], 15 residues [YFP-LBR (1-600)], the last two residues [YFP-LBR (1-613)] or only the last residue [YFP-LBR (1-614) Figure 1 and Table 2]. When transiently expressed in U2OS, all four constructs induced NAVs, CVs, and nuclear compaction (data not shown). Finally, in order to find out what type of amino acid could replace the tyrosine at position 615, we mutagenized it to alanine and phenylalanine,

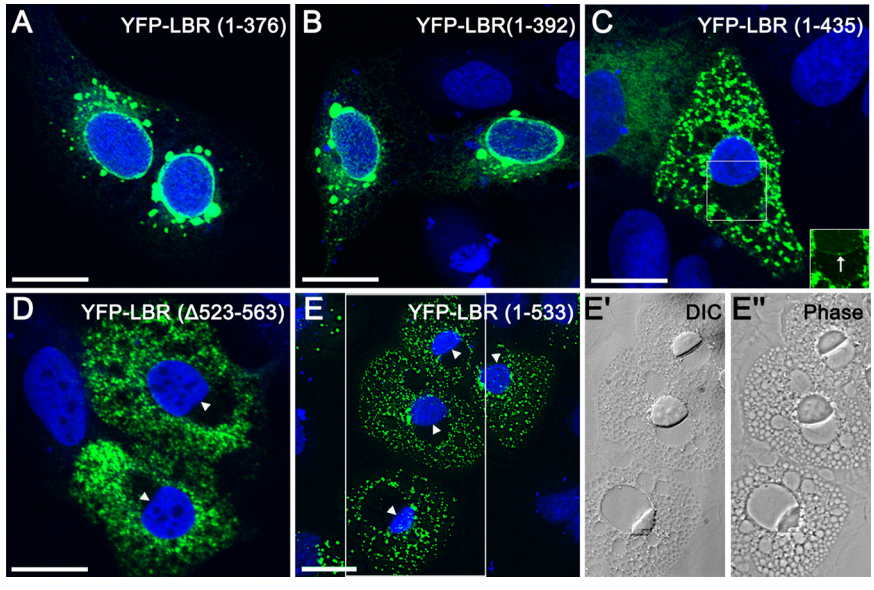


**Figure 4.** Transient expression of five YFP-LBR mutants in human U2OS cells. (A and B) YFP-LBR (1-376) and YFP-LBR (1-392) localize to the nuclear rim and also form aggregates in the cytoplasm, similar to those seen in cells expressing YFP-LBR wt (see Figure 3). Both LBR variants do not alter nuclear morphology. (C–E) Expression of the LBR mutants YFP-LBR (1-435), (Δ523-563), and (1-533) cause the formation of highly compacted nuclei and NAVs that contain no fluorescence signal of the fusion protein. At the interface of the nuclei and these NAVs, nuclei are straight (arrowheads). Furthermore, with all three variants also CVs are formed. Although the mutants seem to localize predominantly in the cytoplasm, some mutant protein can be detected at the nuclear rim (inset in C, arrow). NAVs and CVs appear as very prominent, flat areas in DIC (E′) and as distinct structures in phase contrast microscopy (E″). E′ and E″ represent the field in E designated by the white box. Chromatin was counterstained with DAPI (blue). Original images were collected with a 63× objective. Bar, 20 $\mu$m.

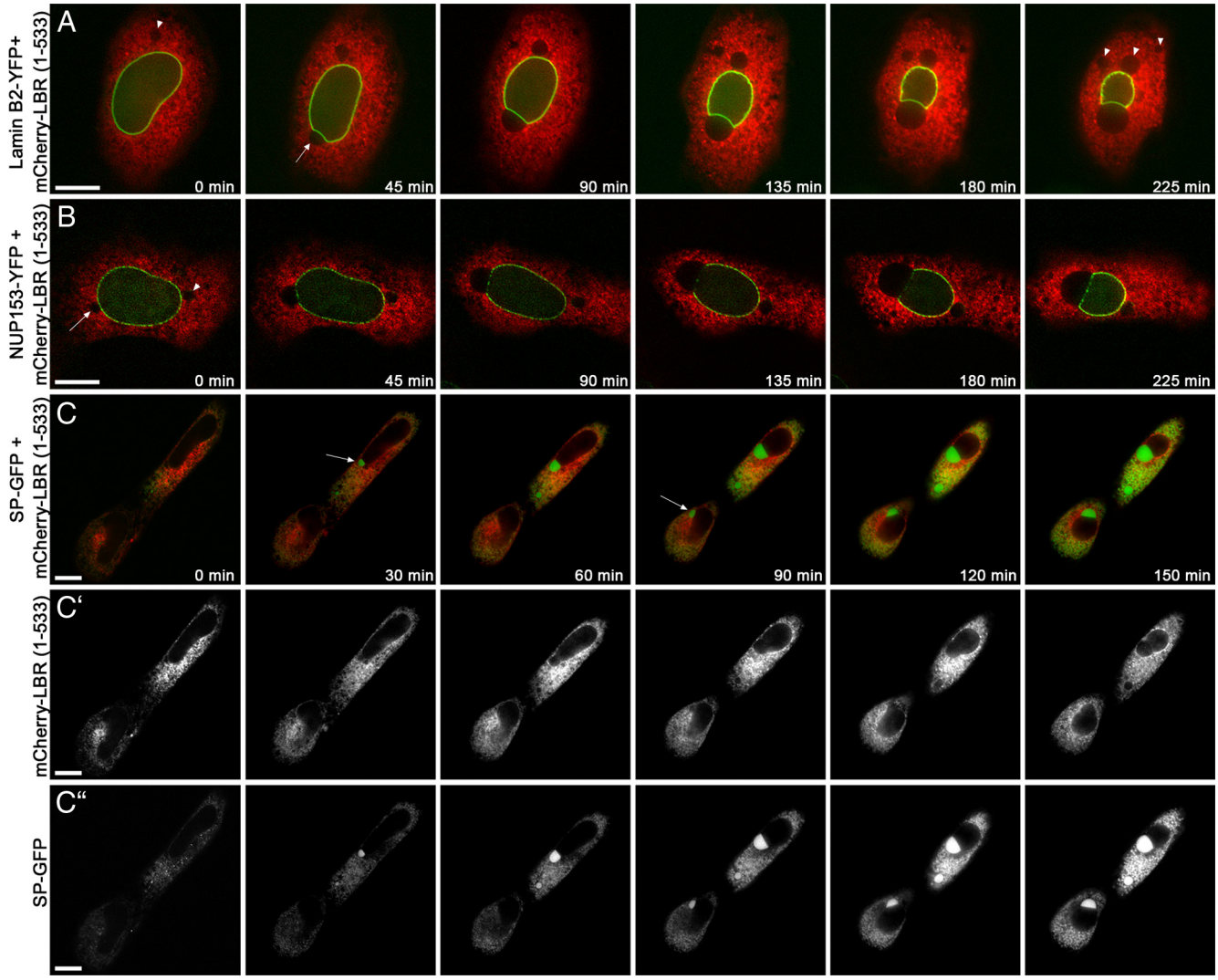


**Figure 5.** Live cell imaging microscopy of U2OS cells 12 h after transient transfection with mCherry-LBR (1-533). (A) U2OS cells stably expressing YFP-lamin B2 as a marker for the nuclear lamina were transfected with mCherry-LBR (1-533). After 12 h, a vacuole is detectable in the cytoplasm without contact to the NE (A, 0 min, arrowhead). During the experiment, more CVs occurred that grew in size (A, 225 min, arrowheads). In addition, one vacuole-like structure in close contact with the NE (A, 45 min, arrow) increased strongly in volume, whereas the nucleus showed a volume reduction over time. (B) U2OS cells stably expressing NUP153-YFP as a marker for the NE were transfected with mCherry-LBR (1-533). Twelve hours after transfection, two small vacuoles are present of which one is stable in size during time (B, 0 min, arrowhead), whereas a second markedly grew and developed to a large NAV (B, 0 min, arrow). After 135 min, most NPCs are absent at the interface between nucleus and the NAV. (C) U2OS cells transiently coexpressing SP-GFP, a marker for the ER lumen, and mCherry-LBR (1-533). Arrows indicate sites where NAVs occur that continuously increase in size. Color channels of C were split in mCherry-LBR (1-533) (C′) and SP-GFP (C″). Arrows and arrowheads indicate NAVs and CVs, respectively. Original images were collected with a 60× objective. Bar, 10 $\mu$m.

respectively. After transfection, YFP-LBR (Y615F) behaved like YFP-LBR wt. In contrast, YFP-LBR (Y615A) provoked the effect with full penetrance (Supplemental Figure S5). In summary, our functional mapping of LBR identified two crucial residues, i.e., E407 and Y615 that are important for the regular function of the human LBR protein. Moreover, we demonstrated that selected changes in these two residues are sufficient to severely affect normal nuclear shape and cell morphology of U2OS cells.

### *Live Cell Imaging Reveals a Contiguous Dilation of the Perinuclear Space and Compaction of Nuclei Starting Early after Transfection*

In transfection experiments with cells fixed 24 h after transfection, we observed cells containing small NAVs, whereas in others, the nuclear volume was decreased to ~20% compared with untransfected cells, and the NAVs adjacent to these nuclei were very large. To investigate the morphological changes in a time-dependent manner, we performed live cell imaging with U2OS cells stably transfected with either YFP-lamin B2 as a marker for the nuclear lamina or with NUP153-YFP as a marker for NPCs. From 12 h on after transfection with mCherry-LBR (1-533), images were collected every 5 min. Up to this time point, U2OS cells usually were still found without CVs, NAVs, and with a regular nuclear shape (Figure 5A and Supplemental Movie S1). Formation of a NAV started with a small vacuole in proximity to the nucleus, which increased in size during the following hours (Figure 5A, 45 min, arrow). During this process, the contact area between NAV and nucleus expanded as a flat

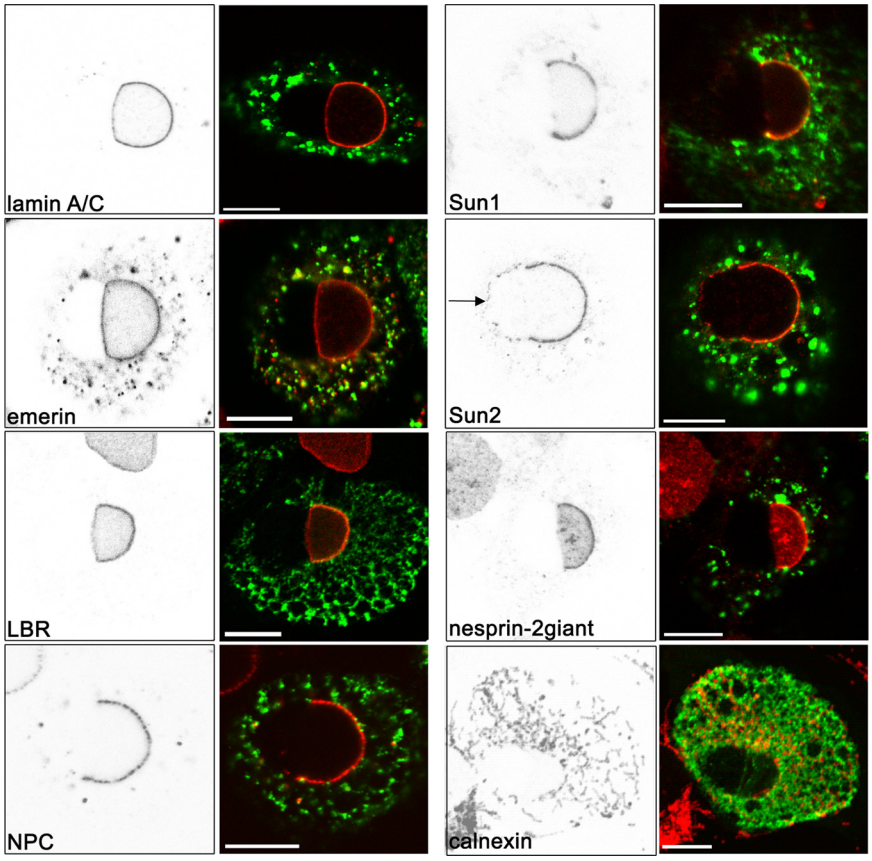


**Figure 6.** Immunofluorescence analysis of various NE and LINC-complex components in U2OS cells transiently expressing the mutant YFP-LBR (1-533). Cells were stained with antibodies as described in the *Materials and Methods* section (left, depicted in inverse gray). Note that the nucleus is on the right side and the adjacent NAV on the left side. In the right panels, merged images of the YFP-LBR (1-533) signal and the corresponding antibody staining (red) are shown. Original images were collected with a 100× objective. Bar, 10 $\mu$m.

plane, and the size of the nucleus decreased in parallel with the growth of the NAV. Furthermore, additional CVs appeared in the cytoplasm (Figure 5A, 225 min, arrowheads). After 225 min, NAV and nucleus were comparable in size. During ongoing compaction of the nucleus, the fluorescence intensity of the nuclear lamina increased significantly, indicating that the total area of the NE was reduced. However, its structure and integrity seemed to be undamaged by the NAV formation.

When imaging a cell line stably expressing NUP153-YFP, particular cells displayed a similar progression from a small vacuole near the nucleus to a large size NAV concomitant with the loss of nuclear volume (Figure 5B and Supplemental Movie S2). Furthermore, we observed a strong effect on the organization of NPCs by the extension of the NAV. Although the NPCs were initially evenly distributed in the NE, they disappeared with time from the interface between the NAV and the nucleus. After 135 min, only a single NPC fluorescence signal was detected in this area. However, at 225 min, NPCs or at least fragments of NPCs were again detected between nucleus and the NAV. These signals might represent newly synthesized NUP components inserted into the nuclear membranes.

Based on these observations, we concluded that the integrity of the NE was heavily disturbed in this area. Furthermore, we hypothesized that the NAV might represent a locally dilated PNS, where INM and ONM had separated from each other, thereby leading to a disruption or a displacement of the NPCs.

To test this hypothesis, we performed live cell imaging of U2OS cells cotransfected with the ER marker SP-GFP and mCherry-LBR (1-533) (Figure 5C and Supplemental Movie S3). SP-GFP is a construct coding for a fusion protein consisting of GFP and the first 21 amino acids of human torsinA, which represent a signal sequence for ER targeting (Liu *et al.*, 2003). The fusion construct is synthesized directly into the ER lumen where it stably remains and eventually also fills up the contiguous PNS. Hence, this construct serves as a marker for the ER and PNS integrity. In the starting situation ~12 h after transfection, we observed only light green tubular staining of the ER lumen and a nonoverlapping red LBR (1-533) signal throughout the cytoplasm. With beginning of NAV formation, SP-GFP appeared in the form of green spot-like signals which occupied the developing NAVs. We also observed the formation of numerous CVs positive for the SP-GFP signal. This strongly supported our assumption that the NAV represents a strongly expanded PNS as a result of separation of INM and ONM over a very large distance. Accordingly, the smaller cytoplasmic vacuoles represent expansions of the ER.

As a control, we coexpressed SP-GFP with mCherry-LBR wt in U2OS cells. The SP-GFP signal revealed a tubular, ER-like pattern, and we never detected any large scale accumulations of the SP-GFP-construct in any cell (Supplemental Figure S4).

In the course of following many cells live over time, we also observed that cells affected by nuclear compaction and NAV and CV formation died within 6–30 h after the first NAVs or CVs were detected.

### *NPCs and the Linker of Nucleoskeleton and Cytoskeleton (LINC) Complex Components Sun1, Sun2, and Nesprin-2 Giant Are Absent from the Interface between Nucleus and the NAV*

Next, we localized hallmark NE proteins in U2OS cells expressing YFP-LBR (1-533) by immunofluorescence microscopy (Figure 6). Staining for lamin A/C revealed it to be distributed to the nuclear side of the NAV. Emerin, a protein that locates at both membranes (Salpingidou *et al.*, 2007),

was indeed partly present at the nuclear rim, but a significant fraction was distributed in a dot-like manner throughout the cytoplasm, too. Some of the emerin signals colocalized with cytoplasmic YFP-LBR (1-533) aggregates, but the majority was spatially separated from sites of mutant LBR aggregation. We never observed this cytoplasmic relocation of emerin in U2OS cells expressing YFP-LBR wt (data not shown). Endogenous LBR was detected with an antibody raised against the C-terminus of the protein, and we found LBR localizing at the nuclear rim with a less strong signal between nucleus and NAV, compared with the remaining NE. Consistent with our live cell imaging observations, NPCs were largely absent between nucleus and the NAV. Sun1 and Sun2 are INM proteins that contain a SUN domain, by which they interact with the KASH-domain of nesprin-1, -2, and -3 within the lumen of the PNS. We detected them at the nuclear rim but they were lacking at the interface between nucleus and NAV (Figure 6). Interestingly, Sun2 protein also localized at the border of the NAV to the cytoplasm, which represents the predicted ONM (arrow). In addition, nesprin-2 giant, an ONM protein, did not localize to any part of the NAV but was present at the remaining NE. In addition, a weak signal was detected within the nucleus. To specifically localize the ER, we stained the ER membrane protein calnexin. We detected signals only outside of the nucleus and the NAV. In summary, we observed that emerin lost its specific NE localization and that SUN proteins, nesprin-2 giant, and NPCs were lacking at the region of the nucleus that flanked the NAV.

### *Ultrastructural Characterization of NAVs and CVs in YFP-LBR (1-533)-transfected Cells*

To verify that INM and ONM segregate and to characterize the structural consequences on both the nuclear and the cytoplasmic side of the NAV, we performed transmission electron microscopy of transfected cells. First, we investigated U2OS cells 10 h after transfection: At this time point, the nuclear internal structure seemed still indistinguishable from nuclei of untransfected cells with typical peripheral heterochromatin and nucleoli of normal size and shape (Figure 7A, compare the upper cell (transfected) to the lower cell (untransfected)). Also, a significant nuclear compaction had not taken place yet. The NE, however, clearly showed a dilation of INM and ONM that surrounded the entire nucleus, in addition to a prominent dilation apparently representing the NAV. At higher magnification, the separation of the INM and ONM at sites where no NAV formed was up to 150 nm (Figure 7, A5, arrow; and A7). At the NAV, the nuclear membranes had a distance of ~4 $\mu$m at the widest point of the dilation, leaving a large region devoid of structures in between them. In contrast, untransfected cells displayed a distance between their nuclear membranes of ~50 nm (see arrowhead in Figure 7A5, and A6). We also observed irregular structures of the single INM, namely, empty membrane loops and structures filled with nucleoplasm or cytoplasm (Figure 7A3). Notably, the presented data corresponds to a very early stage of the membrane phenotype. After 24 h, however, YFP-LBR (1-533)-transfected cells seemed heavily damaged (Figure 7B1). Their cytoplasm was filled with NAVs and CVs. The nuclei were extremely compacted and smaller than the NAVs adjoining them. The chromatin structure seemed strongly condensed, and nucleoli were not detected anymore. The distance between INM and ONM within NAVs was increased up to 10 $\mu$m. Again, a separation of the two membranes over the entire NE was visible (Figure 7B3, B4, B6, and B7).

### *Dilation of the ER Lumen and the PNS Is Not Dependent on the Existence of an Actin or Microtubule Network*

To test whether the cytoskeleton had any influence on the ER and PNS dilations in U2OS cells expressing a NAV-inducing LBR mutant, we treated cells separately with the filament-disrupting compounds latrunculin B and nocodazole, which disrupt actin filaments and microtubules, respectively. Thirty minutes after treatment, the actin network and microtubules were completely destroyed (Figure 8, top). In cells coexpressing mCherry-LBR (1-533) and SP-GFP, the ER and PNS dilations persisted for at least 90 min beyond destruction of the cytoskeletal components, as demonstrated by live cell imaging. Without microtubules, the "cap-like" shape of the dilations even persisted during the entire time of observation. In contrast, upon destruction of the actin network, the shape of the dilated PNS area changed from the characteristic cap-like to ovoid. Strikingly, this effect was reversible: after removal of latrunculin B from the medium, the cap-like shape was restored within 30 min. Hence, we concluded that the cytoskeleton is not responsible for maintaining the dilations of NAVs and CVs. The actin network only influences their shape but not their size.

### *The Related Sterol Reductases TM7SF2 and DHCR7 Display a Comparable Phenotype upon Overexpression*

The domain carrying the disease mutations of LBR shares considerable sequence homology with two other human sterol reductases, TM7SF2 and DHCR7. To test whether the sterol reductase activity was important or even responsible for nuclear compaction and vacuolization, we performed transfection experiments using YFP-tagged wild-type as well as C-terminally truncated versions of TM7SF2 and DHCR7 that correspond to LBR (1-533), LBR (1-435), and LBR (1-392) (Figure 1 and Table 2). When expressed in U2OS cells, all of the C-terminally truncated constructs induced comparable effects to those seen for LBR truncations. Strikingly, already the wild-type version of the proteins caused a marked compaction of nuclei and dilation of the PNS and ER lumen (Figure 9; data not shown).

Because the N-terminal domains of both TM7SF2 and DHCR7 are much shorter than that of LBR, with 12 and 36 amino acids preceding the first transmembrane domain of TM7SF2 and DHCR7, respectively (Figure 1), we wondered whether the YFP-tag might interfere with proper function of the C-terminal domain. Therefore, we generated TM7SF2 wt and TM7SF2 (1-336) without any tag, expressed the constructs in U2OS cells and detected the protein with a TM7SF2-specific antibody. These experiments revealed that even without a tag, TM7SF2 wt and the C-terminal truncated version still induced prominent nuclear compaction and the formation of NAVs (Figure 8, C and D). To investigate whether the LBR N-terminal domain was important for inhibiting the morphological changes we saw with overexpression of TM7SF2 and DHCR7 wild-type, we truncated the LBR N-terminus to the same length of the TM7SF2 and DHCR7 N-termini [YFP-LBR (197-615) and YFP-LBR (173-615)] (Figure 1 and Table 2). When transiently expressed in U2OS, both constructs did not induce nuclear compaction and the formation of NAVs or CVs but instead localized as large aggregates to the cytoplasm and slightly stained the nuclear rim (Figure 8, G and H). In conclusion, we found that overexpression of distinct LBR variants carrying C-terminal truncations and that of the related sterol reductases TM7SF2 and DHCR7 results in the same morphological abnormalities in U2OS cells.

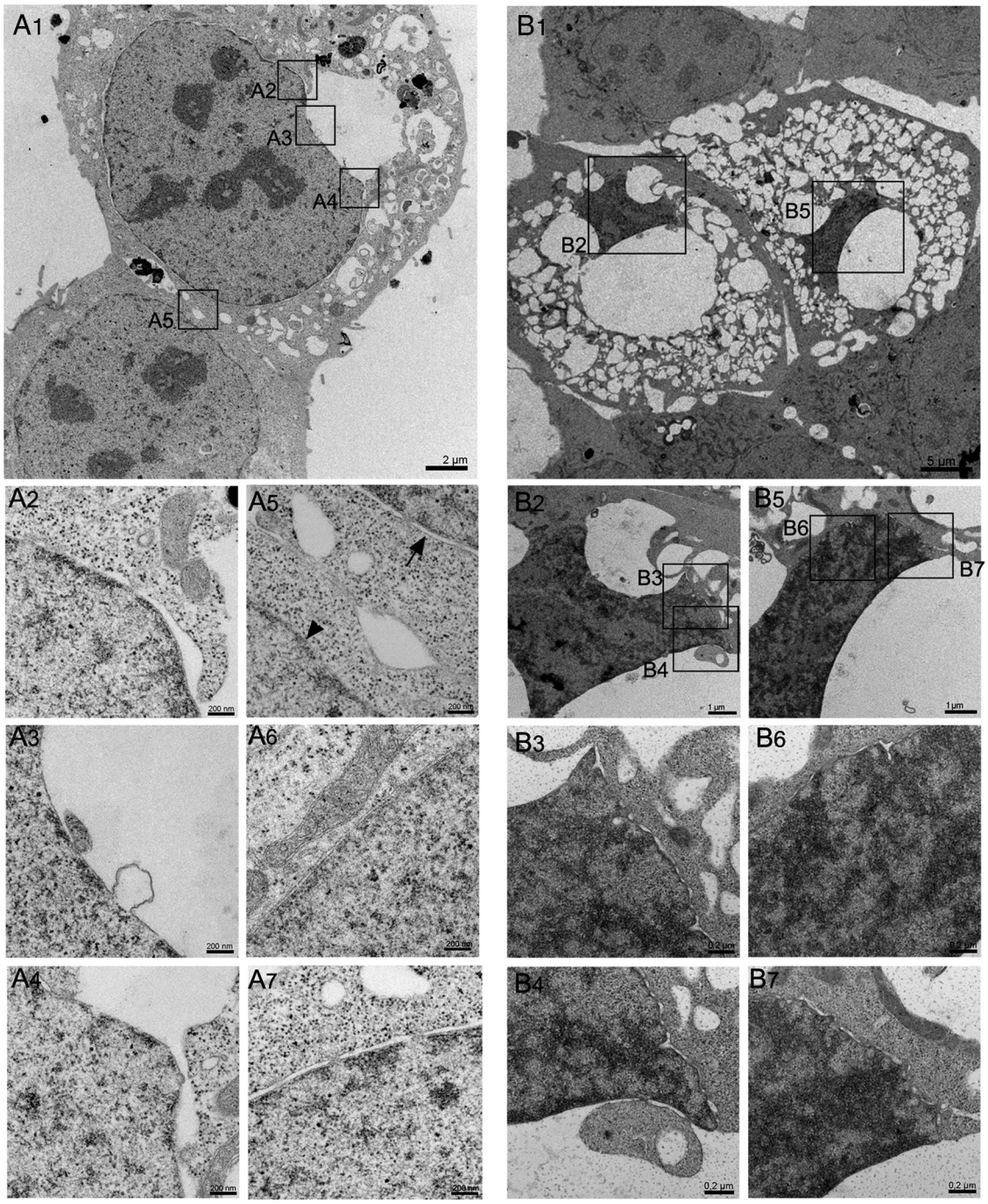


**Figure 7.** Electron microscopy images of ultrathin sections showing U2OS cells transiently expressing the mutant YFP-LBR (1-533) after 10 h (A1–A7) and after 24 h (B1–B7). (A1–A7) After 10 h, nuclei still seem normal in size but display a markedly increased distance of INM and ONM (arrow in A5) compared with the NE of a neighboring untransfected cell (arrowhead in A5). The NAV area comprises 12% of the nuclear area. (A2–5) represent higher magnifications of insets in A1. Dilation of the INM and ONM at the NAV can be clearly detected in (A2) and (A4). A6 and A7 display the NE of a control and a transfected cell, respectively. (B1) Two U2OS cells transiently expressing YFP-LBR (1-533) fixed 24 h after transfection. Nuclei display massive volume loss and large-size NAVs and CVs. The INM and ONM distance within the NAVs is 10 and 7 $\mu$m (A1, left cell and right cell), respectively. The entire cells are filled with vacuoles. Nuclei are enlarged in B2 and B5, higher magnifications of the NE in (B3, B4, B6, and B7). (7B4) Remnants of a normal NE are detected forming a cytoplasm-filled vesicle attached to the nucleus, with an INM and ONM and two NPCs.

### *LBR Mutants Do Not Provoke the Accumulation of Abnormal Cholesterol Intermediates*

To test whether changes in the sterol reductase activity of the transfected proteins were responsible for dilation of the PNS and ER lumen as well as nuclear compaction, we investigated the sterol patterns of each untransfected, YFP-LBR wt, and YFP-LBR (1-533)-transfected U2OS cells (Supplemental Figure S6). This idea was derived from a study that reported elevated levels of an abnormal cholesterol intermediate in a fetus affected with Greenberg skeletal dys-

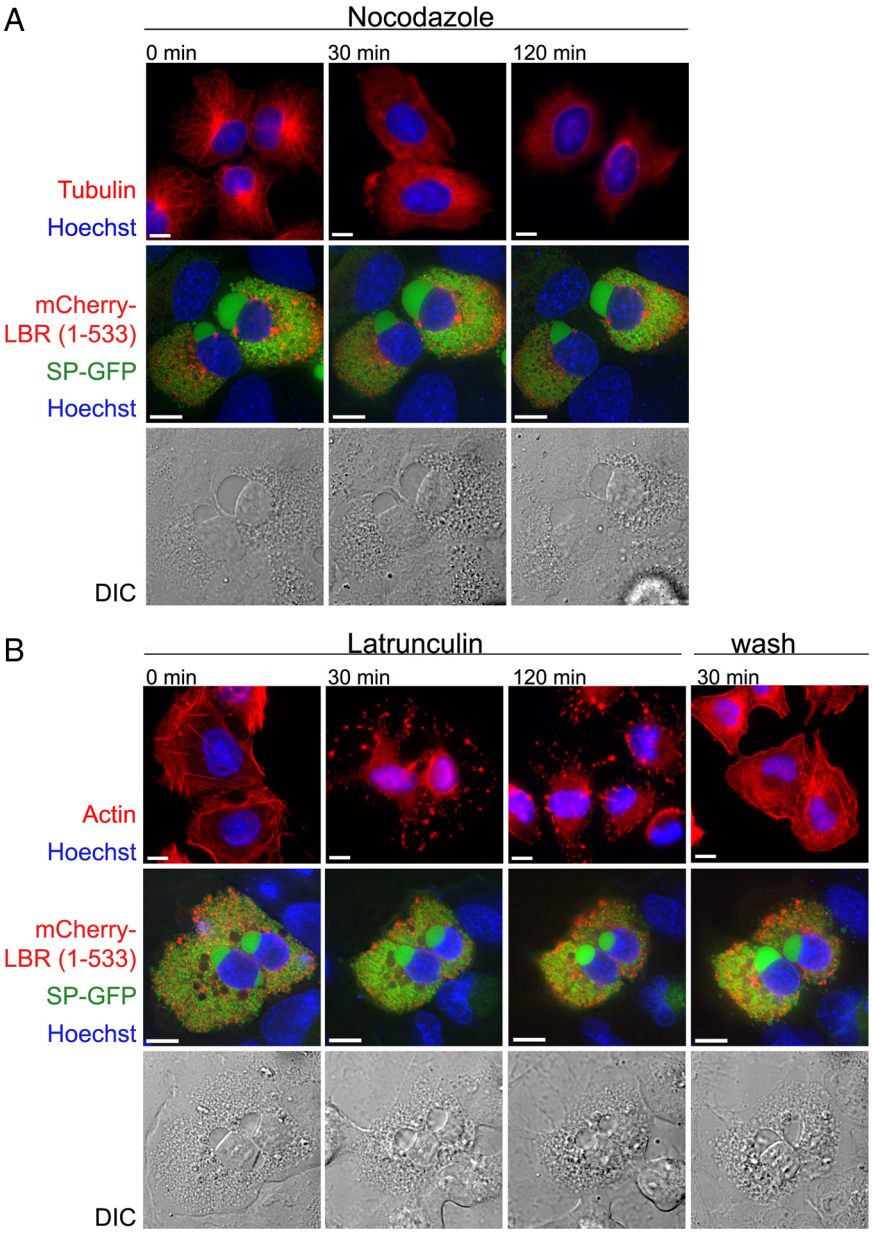


**Figure 8.** Effect of filament-disrupting drugs on NAVs and CVs of U2OS cells. To disrupt microtubules or actin filaments, U2OS cells were treated with nocodazole or latruculin B. Top, U2OS cells treated with nocodazole (A) or latrunculin B (B), fixed after 30 and 120 min and stained for $\alpha$-tubulin or $\beta$-actin. After latrunculin B treatment for 120 min, cells were washed with PBS and maintained in normal growth medium for 30 more minutes and then fixed and stained for $\beta$-actin. Middle, live cell imaging of U2OS cells transiently coexpressing mCherry-LBR (1-533) and SP-GFP as an ER lumenal marker counterstained with the DNA marker Hoechst 33342. Bottom, corresponding DIC micrographs. (A) Despite complete destruction of microtubules, dilated areas of the PNS keep the characteristic, cap-like shape. (B) After disruption of actin filaments, the NAVs remain stable structures within the cell. However, they lose their characteristic, cap-like shape. 120 min after latrunculin B treatment, cells were washed and maintained in normal growth medium. After 30 min, the NAV shape had recovered to the typical, cap-like morphology. Original images were collected with a 60× objective. Bar, 10 $\mu$m.

plasia (Waterham *et al.*, 2003). As in the previous report, lipids were extracted and analyzed by gas chromatography and mass selective detection. In all samples, one main peak was observed with a retention time of 18.6 min, which corresponded to cholesterol. However, no unprocessed cholesterol precursor was detected. Therefore, the presence of mutated or wild-type YFP-LBR did not result in a significant change of sterol composition, and most notably, we demonstrated that no abnormal cholesterol intermediate accumulated in all three experimental situations. We hence conclude that changes in sterol reductase activity of mutated LBR, TM7SF2, or DHCR7 can be neglected to explain the observed effects in U2OS cells.

### *Nuclear Compaction and NAV and CV Formation Are Not Induced by ER Stress, Autophagy, or Apoptosis*

In many cells, the ER lumen comprises ~10% of the total cell volume (Csala *et al.*, 2006). To exclude that unspecific stress responses were causative for the massive volume expansion of the ER and PNS in U2OS cells, we tested transfected cells for ER stress, autophagy, and apoptosis. Massive cellular production of an introduced gene can cause a cellular stress response, e.g., the activation of the unfolded protein response (UPR). UPR is the major signaling pathway for the ER-associated degradation pathway (ERAD) but is critically involved in ER-activated autophagy (ERAA) as well (Ding and Yin, 2008). Interestingly, the massive overexpression of YFP-LBR wt leads to large accumulations of the fusion protein in U2OS cells in the form of stacked membrane arrays termed OSER structures (Snapp *et al.*, 2003). However, these structures do not interfere with cellular processes, as U2OS cell lines stably expressing YFP-LBR wt frequently display these structures (Supplemental Figure S1). Theoretically, the overexpression of mutated LBR might lead to folding problems and activation of ERAD or ERAA. Nevertheless, both pathways were not activated in U2OS cells exhibiting com-

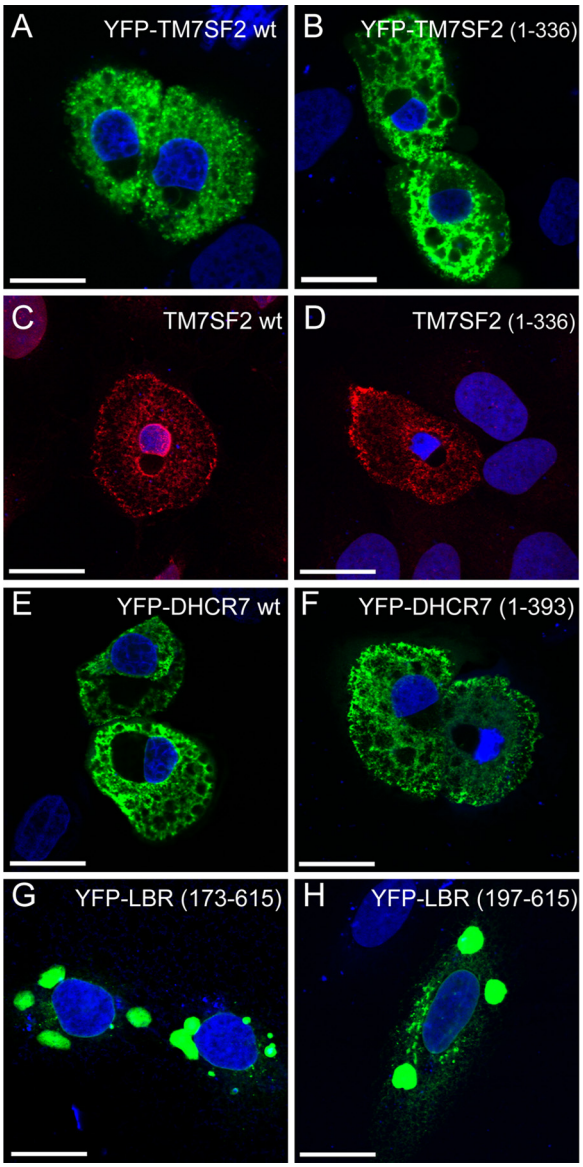


**Figure 9.** Expression of wild-type and C-terminally truncated TM7SF2 and DHCR7 and N-terminally truncated LBR: (A and B) YFP-tagged TM7SF2 wt and the C-terminal truncation YFP-TM7SF2 (1-336) lead to compaction of the nucleus with development of NAVs. (C and D) Expression of TM7SF2 wild-type and TM7SF2 (1-336) in U2OS cells also induced these effects, indicating that they were independent of the fluorescent tag. Transfected cells are recognized by the amount of protein as detected by antibody staining. (E and F) YFP-DHCR7 wt and YFP-DHCR7 (1-393) also induce the described phenotype. Note that all mutant constructs of TM7SF2 and DHCR7 presented in Figure 1 and Table 2 induced nuclear compaction, NAV and CV formation (data not shown). (G and H) YFP-LBR N-terminal truncations with corresponding length of the TM7SF2 and DHCR7 N-termini (12 and 36 aa, respectively) form aggregates within the cytoplasm but do not affect cellular morphology. Chromatin was counterstained with DAPI. Original images were collected with a 100× objective. Bar, 20 $\mu$m.

pacted nuclei and ER and PNS lumenal expansion, as confirmed by analysis of Xbp1 mRNA as an ER stress marker (Kaser *et al*., 2008) and of the autophagy marker protein LC3 (Supplemental Figure S7).

We also tested affected U2OS cells for apoptosis, as dilated ER and vacuolized cytoplasm is a reported hallmark of cells undergoing programmed cell death (Hacker, 2000). Using a terminal deoxynucleotidyl transferase dUTP nick-end labeling (TUNEL) assay, we demonstrated that cells did not undergo apoptosis even after the ER and NE were already dilated. Hence, expansion of the ER lumen and PNS was not a phenotypic manifestation of an apoptotic event (Supplemental Figure S8). We finally examined the transcriptional activity of U2OS cells exhibiting nuclear membrane dilation. For this purpose, we grew U2OS cells 24 h after transfection with YFP-LBR wt or YFP-LBR (1-533) for 4 h in the presence of 5-fluorouridine (5-FU). 5-FU is cell permeable, becomes intracellularly phosphorylated, and is then incorporated into newly synthesized RNA, where it can be detected using specific BrdU antibodies (Vidair and Rubin, 2005; So *et al*., 2009). We clearly detected 5-FU labeled RNA transcripts in nuclei from YFP-LBR wt-transfected cells, and to a similar extend in YFP-LBR (1-533)-transfected cells, despite the compacted state of chromatin in the latter case (Supplemental Figure 9). Therefore, U2OS cells exhibiting dilation of INM and ONM as well as compacted nuclei are still transcriptionally active. RNA transcripts were not detected after RNase digestion of fixed cells, or in cells incubated in actinomycin D (a well established inhibitor of transcription) 4 h before 5-FU incorporation, indicating that the anti-BrdU antibody specifically recognized 5-FU incorporated into nascent RNA. All cells exhibiting compacted nuclei showed transcriptional activity.

## DISCUSSION

The ER is continuous with the INM and ONM. This highly dynamic, interconnected membrane system is composed of polygonal arrays of tubules and sheet-like cisternae. The thickness of an ER sheet, the diameter of a tubule and the distance between INM and ONM is remarkably constant in various cells (Shibata *et al*., 2006). In this study, we have demonstrated that overexpression of distinct LBR C-terminal mutations and intact TM7SF2 and DHCR7 leads to a novel, as yet undescribed cellular phenotype: the ER lumen and the PNS lose their normal tubular or sheet-like morphology and progressively develop large dilations throughout the entire cell and specifically at the nuclear periphery.

### *Mutant LBR Induces Nuclear Compaction, Segregation of Nuclear Membranes, and Vacuolization of the ER*

In affected cells, the entire NE revealed a separation between the INM and ONM, leading to an enlargement of the distance to 50–150 nm, compared with 30–50 nm in normal cells. In distinct areas of the NE, the two membranes were not only disconnected, but additionally heavily dilated. The enlarged PNS in between them appeared as a compartment that we named NAV. Interestingly, several components of the NE, namely, the NPCs, nesprin-2 giant and SUN proteins, were absent in the membranes surrounding the NAV, whereas they were present within the remaining NE. Concomitant with the dilation of ER and nuclear membranes, nuclei compacted markedly and CVs developed and increased in size. These structures probably represent either single vacuoles or dilated areas within an ER tubule.

The cell lines used in this study originated from different tissues. Some cell lines responded very strongly and died as a result of overexpression (U2OS, T98G, and A431), whereas others responded weakly or not at all to the expression of mutant LBR (MCF7, HeLa, and PLC). Each of these cell lines most likely expresses a unique set of tissue-specific genes, but they may also vary markedly in their expression of housekeeping genes, as demonstrated here for the lamin and

LBR levels in Figure 2. Based on proteomic analysis on liver cells, around 80 integral NE proteins are estimated to exist (Schirmer *et al*., 2003). Hence, the variability in NE components can vary significantly among different cell types. The different responsiveness of cells toward LBR mutant variants may therefore reflect differences in their NE proteome.

Variability in the reaction of cell lines further indicates that the mutated LBR variants are not toxic by themselves but that their toxicity is dependent on distinct cellular properties that determine their susceptibility. We also found that overexpression of the wild-type forms of TM7SF2 and DHCR7 but not wt LBR mimicked the phenotype observed for mutant LBR. Hence, even fully functional proteins can critically affect the ER and NE morphology.

### *Progression from a Regular NE Sheet and ER Cisternae toward a Highly Expanded Compartment*

To explain the large-scale dilations of the lumenal system constituted in the ER and the PNS, one has to understand the molecular elements that determine the structure of this compartment. A possible candidate for shaping regular ER morphology is the cytoskeleton linking membrane protein Climp-63, an ER membrane protein that is not present in the NE. It has a large coiled-coil lumenal domain that forms ~90-nm-long rods that are long enough to span the ER lumen and might thus contribute to ER morphology by the formation of a lumenal protein scaffold (Klopfenstein *et al*., 2001). At the NE, the most probable candidates are nesprins and SUN proteins, components of the so-called LINC complex, that interact with each other within the lumen and thus link the two membranes together (Razafsky and Hodzic, 2009). It was indeed demonstrated previously that Sun1 and Sun2 depletion from HeLa cells or the truncation of the N-terminal chromatin binding domain of Sun1 frequently led to increased disjunction of the INM and ONM, with partially expanded PNS (Crisp *et al*., 2006; Xiong *et al*., 2008). In addition, knockdown of nesprin-1$\alpha$ in U2OS cells resulted in a local and limited separation of INM and ONM (Zhang *et al*., 2007).

With mutant LBR expression, we have observed loss of Sun1, Sun2, nesprin-2 giant, and of NPCs at the NAVs. It is not clear whether their depletion represents an initial step leading to membrane disconnection or whether these proteins get lost as a consequence of membrane dilation. Moreover, there is one remarkable difference between the INM and ONM separation we observed upon expression of mutant LBR, compared with the cases mentioned above. In those studies, the INM and ONM never dilated over such a large distance as seen in the cell lines reported here. In addition, the remarkable ER lumenal expansion and the nuclear compaction have not been observed elsewhere.

### *Dual Effects: Nuclear Compaction and Vacuolization of the Cytoplasm*

We hypothesize that LBR mutant variants primarily affect the integrity of the lumenal compartment consisting of the ER and the PNS and that these mutants only indirectly influence nuclear structure. This hypothesis is underlined by the finding that the related sterol reductases TM7SF2 and DHCR7 induce a comparable phenotype. These two proteins are predicted to reside in the cytoplasm and are not believed to be in prolonged direct physical contact with chromatin (Holmer *et al*., 1998). Moreover, our live cell imaging experiments revealed that severe nuclear compaction always occurred during NAV formation and that the increase of NAV volume temporally and spatially correlated with the loss of nuclear size. Hence, NAV formation preceded nuclear compaction. Accordingly, we never observed compacted nuclei in the absence of a NAV. Following this thought, loss of various NE components from the NAV membranes might be a consequence of membrane dilation.

Although we favor the idea of membrane dilation as initial event, we cannot exclude that mutant LBR directly induces chromatin condensation in affected cells. LBR is a major element to couple chromatin to the NE and is critically involved in organizing heterochromatin at the nuclear periphery (Gruenbaum *et al*., 2005; Zwerger *et al*., 2008). Hence, high levels of mutant LBR may strongly promote heterochromatin formation and lead to nuclear compaction. Expansion of the PNS and the peripheral ER lumen may then be a result of altered gene transcription activities affecting the synthesis of proteins needed for proper ER function.

### *Molecular Mechanisms Underlying ER and PNS Expansion*

We found that not only C-terminal truncations but even single amino acid changes within the full length LBR (namely, mutations of E407 and Y615 to alanine) are sufficient to induce ER lumen and PNS expansion as well as compaction of the nucleus. In contrast, the mutation of Y615 to phenylalanine did not induce NAV formation, suggesting that loss of a potential phosphorylation site (tyrosine) is not a likely explanation. Complete loss of the last amino acid was sufficient to cause the phenotype. This implies that the effect on the lumen occurs due to distinct alterations in the LBR structure or of its function.

The molecular mechanism that leads to the remarkable membrane extension remains elusive. So far, we have shown that neither ER stress activation, autophagy, nor apoptosis induced the observed phenotype. In addition, there was no correlation with the endogenous content of LBR or lamins. Because the sterol content of YFP-LBR (1-533) expressing cells was not altered compared with untransfected cells, it seems unlikely that the sterol reductase activity is causative for the cellular morphological abnormalities. However, the applied sterol analysis has inherent limitations, namely, detection of subtile changes of the sterol content. We hence cannot exclude the possibility that minor changes in cholesterol concentration of ER and NE membranes or the presence of low amounts of intermediate sterol products might affect membrane properties and function.

Alternatively, truncated LBR variants might interfere with ER proteins and NE components belonging to the LINC complex as mentioned above. However, we observed not only a disruption of ER and NE membranes but also a lumenal expansion leading to PNS dilations up to 10 $\mu$m. As demonstrated by electron microscopy, 24 h after transfection NAVs and CVs occupy the entire cytoplasm. Therefore, a disruption of ER and NE membranes might not sufficiently explain the extensive growth of NAVs and CVs. The presence of mutant LBR or wild-type TM7SF2 and DHCR7 might also alter membrane properties, e.g., membrane fluidity or permeability. A wide spectrum of functional consequences can be envisioned. For example, ion currents across the membrane could be altered, thereby leading to osmotic or signaling consequences. NAVs and CVs are stable structures that do not collapse upon destruction of the actin filament or microtubule network. This suggests that membrane dilation may be a result of a buildup of a turgor within the lumen and are not caused by cytoskeletal forces or by the uncoupling of SUN/KASH complexes.

In summary, we suppose that either transport or osmotic processes across the membrane are altered, leading to the deposition of aqueous or any cellular material from the

cytoplasm and nucleoplasm into the ER lumen. This process would cause loss of nuclear volume concomitant with the dilation of the ER lumen and the PNS as a consequence of massive increase in its content.

## CONCLUSIONS

So far, the N-terminal domain of LBR has been the primary topic of research and discussion. The present study provides evidence that the C-terminal domain has a fundamental influence on the ER and NE morphology. The regular spacing of the ER and NE sheets and tubules is obviously challengeable by alterations in this C-terminal domain, eventually leading to cell death. Further studies are needed to elucidate interactions of this domain and to examine whether it has additional functions, other than sterol reductase activity.

## ACKNOWLEDGMENTS

We thank Rita Roberti, Didier Hodzic, Angelika Noegel, Birthe Fahrenkrog, Stephanie Geiger, Christine Dreger, and Otto Mannherz for kindly providing us with antibodies or plasmids and Nadine Sachs for excellent technical support. We greatly acknowledge the collaboration with Hanswalter Zentgraf. We gratefully thank Katrin Hoffmann, Donald E. Olins and Ada L. Olins for critical review of the manuscript and discussion of this work. This work was supported by European Union's FP6 Life Science, Genomics and Biotechnology for Health area (LSHM-CT-2005-018690 to H. H. and M. Z.).

## REFERENCES

Bennati, A. M., Castelli, M., Della Fazia, M. A., Beccari, T., Caruso, D., Servillo, G., and Roberti, R. (2006). Sterol dependent regulation of human TM7SF2 gene expression: role of the encoded 3beta-hydroxysterol Delta14-reductase in human cholesterol biosynthesis. Biochim. Biophys. Acta *1761*, 677–685.

Bennati, A. M., *et al*. (2008). Disruption of the gene encoding 3beta-hydroxysterol Delta-reductase (Tm7sf2) in mice does not impair cholesterol biosynthesis. FEBS J. *275*, 5034–5047.

Best, S., Salvati, F., Kallo, J., Garner, C., Height, S., Thein, S. L., and Rees, D. C. (2003). Lamin B-receptor mutations in Pelger-Huet anomaly. Br. J. Haematol. *123*, 542–544.

Bradford, M. M. (1976). A rapid and sensitive method for the quantitation of microgram quantities of protein utilizing the principle of protein-dye binding. Anal. Biochem. *72*, 248–254.

Campbell, R. E., Tour, O., Palmer, A. E., Steinbach, P. A., Baird, G. S., Zacharias, D. A., and Tsien, R. Y. (2002). A monomeric red fluorescent protein. Proc. Natl. Acad. Sci. USA *99*, 7877–7882.

Cohen, T. V., Klarmann, K. D., Sakchaisri, K., Cooper, J. P., Kuhns, D., Anver, M., Johnson, P. F., Williams, S. C., Keller, J. R., and Stewart, C. L. (2008). The lamin B receptor under transcriptional control of C/EBPepsilon is required for morphological but not functional maturation of neutrophils. Hum. Mol. Genet. *17*, 2921–2933.

Crisp, M., Liu, Q., Roux, K., Rattner, J. B., Shanahan, C., Burke, B., Stahl, P. D., and Hodzic, D. (2006). Coupling of the nucleus and cytoplasm: role of the LINC complex. J. Cell Biol. *172*, 41–53.

Csala, M., Banhegyi, G., and Benedetti, A. (2006). Endoplasmic reticulum: a metabolic compartment. FEBS Lett. *580*, 2160–2165.

Ding, W. X., and Yin, X. M. (2008). Sorting, recognition and activation of the misfolded protein degradation pathways through macroautophagy and the proteasome. Autophagy *4*, 141–150.

Dreger, C. K., Konig, A. R., Spring, H., Lichter, P., and Herrmann, H. (2002). Investigation of nuclear architecture with a domain-presenting expression system. J. Struct. Biol. *140*, 100–115.

Dwyer, N., and Blobel, G. (1976). A modified procedure for the isolation of a pore complex-lamina fraction from rat liver nuclei. J. Cell Biol. *70*, 581–591.

Ellenberg, J., Siggia, E. D., Moreira, J. E., Smith, C. L., Presley, J. F., Worman, H. J., and Lippincott-Schwartz, J. (1997). Nuclear membrane dynamics and reassembly in living cells: targeting of an inner nuclear membrane protein in interphase and mitosis. J. Cell Biol. *138*, 1193–1206.

Fitzky, B. U., Witsch-Baumgartner, M., Erdel, M., Lee, J. N., Paik, Y. K., Glossmann, H., Utermann, G., and Moebius, F. F. (1998). Mutations in the Delta7-sterol reductase gene in patients with the Smith-Lemli-Optiz Syndrome. Proc. Natl. Acad. Sci. USA *95*, 8181–8186.

Gajewski, A., and Krohne, G. (1999). Subcellular distribution of the *Xenopus* p58/lamin B receptor in oocytes and eggs. J. Cell Sci. *112*, 2583–2596.

Geiger, S. K., *et al*. (2008). Incomplete nonsense-mediated decay of mutant lamin A/C mRNA provokes dilated cardiomyopathy and ventricular tachycardia. J. Mol. Med. *86*, 281–289.

Gruenbaum, Y., Margalit, A., Goldman, R. D., Shumaker, D. K., and Wilson, K. L. (2005). The nuclear lamina comes of age. Nat. Rev. Mol. Cell Biol. *6*, 21–31.

Guarda, A., Bolognese, F., Bonapace, I. M., and Badaracco, G. (2009). Interaction between the inner nuclear membrane lamin B receptor and the heterochromatic methyl binding protein, MeCP2. Exp. Cell Res. *315*, 1895–1903.

Hacker, G. (2000). The morphology of apoptosis. Cell Tissue Res. *301*, 5–17.

Hoffmann, K., *et al*. (2002). Mutations in the gene encoding the lamin B receptor produce an altered nuclear morphology in granulocytes (Pelger-Huet anomaly). Nat. Genet. *31*, 410–414.

Holmer, L., Pezhman, A., and Worman, H. J. (1998). The human lamin B receptor/sterol reductase multigene family. Genomics *54*, 469–476.

Kaser, A. *et al*. (2008). XBP1 links ER stress to intestinal inflammation and confers genetic risk for human inflammatory bowel disease. Cell *134*, 743–756.

Klopfenstein, D. R., Klumperman, J., Lustig, A., Kammerer, R. A., Oorschot, V., and Hauri, H. P. (2001). Subdomain-specific localization of CLIMP-63 (p63) in the endoplasmic reticulum is mediated by its luminal alpha-helical segment. J. Cell Biol. *153*, 1287–1300.

Laemmli, U. K. (1970). Cleavage of structural proteins during the assembly of the head of bacteriophage T4. Nature *227*, 680–685.

Liu, Z., Zolkiewska, A., and Zolkiewski, M. (2003). Characterization of human torsinA and its dystonia-associated mutant form. Biochem. J. *374*, 117–122.

Lusk, C. P., Blobel, G., and King, M. C. (2007). Highway to the inner nuclear membrane: rules for the road. Nat. Rev. Mol. Cell Biol. *8*, 414–420.

Martins, S. B., Eide, T., Steen, R. L., Jahnsen, T., Skalhegg, B. S., and Collas, P. (2000). HA95 is a protein of the chromatin and nuclear matrix regulating nuclear envelope dynamics. J. Cell Sci. *113*, 3703–3713.

Oosterwijk, J. C., Mansour, S., van Noort, G., Waterham, H. R., Hall, C. M., and Hennekam, R. C. (2003). Congenital abnormalities reported in Pelger-Huet homozygosity as compared to Greenberg/HEM dysplasia: highly variable expression of allelic phenotypes. J. Med. Genet. *40*, 937–941.

Porter, F. D. (2008). Smith-Lemli-Opitz syndrome: pathogenesis, diagnosis and management. Eur. J. Hum. Genet. *16*, 535–541.

Pyrpasopoulou, A., Meier, J., Maison, C., Simos, G., and Georgatos, S. D. (1996). The lamin B receptor (LBR) provides essential chromatin docking sites at the nuclear envelope. EMBO J. *15*, 7108–7119.

Razafsky, D., and Hodzic, D. (2009). Bringing KASH under the SUN: the many faces of nucleo-cytoskeletal connections. J. Cell Biol. *186*, 461–472.

Roberti, R., Bennati, A. M., Galli, G., Caruso, D., Maras, B., Aisa, C., Beccari, T., Della Fazia, M. A., and Servillo, G. (2002). Cloning and expression of sterol Delta 14-reductase from bovine liver. Eur. J. Biochem. *269*, 283–290.

Salpingidou, G., Smertenko, A., Hausmanowa-Petrucewicz, I., Hussey, P. J., and Hutchison, C. J. (2007). A novel role for the nuclear membrane protein emerin in association of the centrosome to the outer nuclear membrane. J. Cell Biol. *178*, 897–904.

Schirmer, E.C., Florens, L., Guan, T., Yates, J. R., 3rd, and Gerace, L. (2003). Nuclear membrane proteins with potential disease links found by subtractive proteomics. Science *301*, 1380–1382.

Shaner, N. C., Campbell, R. E., Steinbach, P. A., Giepmans, B. N., Palmer, A. E., and Tsien, R. Y. (2004). Improved monomeric red, orange and yellow fluorescent proteins derived from *Discosoma* sp. red fluorescent protein. Nat. Biotechnol. *22*, 1567–1572.

Shibata, Y., Voeltz, G. K., and Rapoport, T. A. (2006). Rough sheets and smooth tubules. Cell *126*, 435–439.

Silve, S., Dupuy, P. H., Ferrara, P., and Loison, G. (1998). Human lamin B receptor exhibits sterol C14-reductase activity in *Saccharomyces cerevisiae*. Biochim. Biophys. Acta *1392*, 233–244.

Snapp, E. L., Hegde, R. S., Francolini, M., Lombardo, F., Colombo, S., Pedrazzini, E., Borgese, N., and Lippincott-Schwartz, J. (2003). Formation of stacked ER cisternae by low affinity protein interactions. J. Cell Biol. *163*, 257–269.

So, L. K., Cheung, S. K., Ma, H. L., Chen, X. P., Cheng, S. H., and Lam, Y. W. (2009). In situ labeling of transcription sites in marine medaka. J. Histochem. Cytochem. (in press).

Soullam, B., and Worman, H. J. (1993). The amino-terminal domain of the lamin B receptor is a nuclear envelope targeting signal. J. Cell Biol. *120*, 1093–1100.

Soullam, B., and Worman, H. J. (1995). Signals and structural features involved in integral membrane protein targeting to the inner nuclear membrane. J. Cell Biol. *130*, 15–27.

Stewart, C. L., Roux, K. J., and Burke, B. (2007). Blurring the boundary: the nuclear envelope extends its reach. Science *318*, 1408–1412.

Veen, M., Stahl, U., and Lang, C. (2003). Combined overexpression of genes of the ergosterol biosynthetic pathway leads to accumulation of sterols in *Saccharomyces cerevisiae*. FEMS Yeast Res. *4*, 87–95.

Vidair, C., and Rubin, H. (2005). Mg2t as activator of uridine phosphorylation in coordination with other cellular responses to growth factors. Proc. Natl. Acad. Sci. USA *102*, 662–666.

Wagner, N., Weber, D., Seitz, S., and Krohne, G. (2004). The lamin B receptor of *Drosophila melanogaster*. J. Cell Sci. *117*, 2015–2028.

Wassif, C. A., Brownson, K. E., Sterner, A. L., Forlino, A., Zerfas, P. M., Wilson, W. K., Starost, M. F., and Porter, F. D. (2007). HEM dysplasia and ichthyosis are likely laminopathies and not due to 3beta-hydroxysterol Delta14-reductase deficiency. Hum. Mol. Genet. *16*, 1176–1187.

Waterham, H. R., Koster, J., Mooyer, P., Noort Gv, G., Kelley, R. I., Wilcox, W. R., Wanders, R. J., Hennekam, R. C., and Oosterwijk, J. C. (2003). Autosomal recessive HEM/Greenberg skeletal dysplasia is caused by 3 beta-hydroxysterol delta 14-reductase deficiency due to mutations in the lamin B receptor gene. Am. J. Hum. Genet. *72*, 1013–1017.

Worman, H. J., and Bonne, G. (2007). "Laminopathies": a wide spectrum of human diseases. Exp. Cell Res. *313*, 2121–2133.

Worman, H. J., Yuan, J., Blobel, G., and Georgatos, S. D. (1988). A lamin B receptor in the nuclear envelope. Proc. Natl. Acad. Sci. USA *85*, 8531–8534.

Xiong, H., Rivero, F., Euteneuer, U., Mondal, S., Mana-Capelli, S., Larochelle, D., Vogel, A., Gassen, B., and Noegel, A. A. (2008). *Dictyostelium* Sun-1 connects the centrosome to chromatin and ensures genome stability. Traffic *9*, 708–724.

Ye, Q., Callebaut, I., Pezhman, A., Courvalin, J. C., and Worman, H. J. (1997). Domain-specific interactions of human HP1-type chromodomain proteins and inner nuclear membrane protein LBR. J. Biol. Chem. *272*, 14983–14989.

Ye, Q., and Worman, H. J. (1994). Primary structure analysis and lamin B and DNA binding of human LBR, an integral protein of the nuclear envelope inner membrane. J. Biol. Chem. *269*, 11306–11311.

Zacharias, D. A., Violin, J. D., Newton, A. C., and Tsien, R. Y. (2002). Partitioning of lipid-modified monomeric GFPs into membrane microdomains of live cells. Science *296*, 913–916.

Zhang, Q., *et al*. (2007). Nesprin-1 and -2 are involved in the pathogenesis of Emery Dreifuss muscular dystrophy and are critical for nuclear envelope integrity. Hum. Mol. Genet. *16*, 2816–2833.

Zwerger, M., Herrmann, H., Gaines, P., Olins, A. L., and Olins, D. E. (2008). Granulocytic nuclear differentiation of lamin B receptor-deficient mouse EPRO cells. Exp. Hematol. *36*, 977–987.